A Numerical Scheme to Treat the Open Lateral Boundary of a Limited Area Model

YOSHIO KURIHARA AND MORRIS A. BENDER

Geophysical Fluid Dynamics Laboratory/NOAA, Princeton University, Princeton, NJ 08540

(Manuscript received 21 May 1982, in final form 8 December 1982)

ABSTRACT

A numerical scheme to treat the open lateral boundary of a limited-area primitive equation model was formulated. Although overspecification of the boundary condition is inevitable in the pointwise boundary setting, the scheme was designed to keep the overspecification to a minimum degree. To impose the boundary conditions, a damping technique was used. Special care was taken to deal with the boundary layer winds at the lateral boundary. The above scheme is most suitable when gravity waves do not prevail in the vicinity of the open boundary.

The scheme was tested in the numerical integrations of prognostic equations for a Haurwitz-type wave. Experimental results are presented which indicate the utility of the proposed method.

1. Introduction

An appropriate specification of lateral boundary conditions is one of the crucial factors for a successful time integration of limited-area prediction models. Numerous studies have been conducted to investigate the impact of boundary conditions on the model performance, and various techniques have been used to make undesirable effects minimal (e.g., see the review by Sundström and Elvius, 1979). In this paper, we propose a boundary setting which can be applied under certain circumstances to a limited-area, multilevel primitive equation (PE) model.

It is known that a limited-area prediction by a baroclinic PE model with conventional boundary conditions, by which values of certain variables are specified at each boundary gridpoint, is not a mathematically well-posed problem (e.g., Elvius, 1977; Sundström, 1977). In such a model, the intrinsic phase speeds of the various internal gravity waves present are different—the phase speed for certain vertical modes may be larger than the local wind speed and those for the other modes may be smaller (Elvius, 1977; Klemp and Lilly, 1978). Accordingly, the proper number of variables to be specified at a certain boundary point for some modes may well be improper for other modes. Thus, if the boundary conditions are prescribed pointwise, the number of conditions is not necessarily correct for all modes. Although the overspecification may be avoided by the split treatment of individual vertical modes (Hack and Schubert, 1981), the situation becomes further complicated when the effect of viscosity is included (Sundström, 1977). It should be noted that the split treatment of individual horizontal modes was suggested earlier by Béland and Warn (1975) in dealing with laterally propagating Rossby waves.

Despite the above-mentioned difficulty, acceptable pointwise settings of boundary conditions have been sought. Chen (1973), Chen and Miyakoda (1974) and Miyakoda and Rosati (1977) showed that all variables may be specified at the boundary, if they are approximately compatible to the difference equations. In this case, the strain of overspecification can be relaxed by local smoothing. However, the propriety of the boundary values is not always known. Elvius (1977) stated that the overspecification should be avoided as much as possible. In the present work, we took his suggestion.

There can be many different approaches to the problem of a practical boundary setting. A common goal is to construct a scheme which establishes smooth fields near the boundary without causing a noticeable erroneous impact on solutions in the interior domain. The following are a few strategic matters which are considered to be useful in the formulation of boundary schemes.

1) Certain assumptions may have to be made concerning the time change of fields in the vicinity of the boundaries. In some cases, the change is mainly due to the propagation of a certain predominant wave. In other cases, it is caused by the combination of many waves, for which the representative phase velocity can be defined locally (Orlanski, 1976) or for a vertical column (Klemp and Lilly, 1978). Using the idea of Orlanski (1976), one can apply the inflow and the outflow conditions discriminately to each boundary point on the basis of a duly determined local propagation property.

2) In some models, a dynamical relationship between variables may be postulated near the boundary (e.g., Busalacchi and O'Brien, 1980). This serves to limit the overspecification.

3) Boundary conditions can be imposed gradually so that a possible noise source due to an abrupt change of a field can be tempered.

In this paper, we formulate a new boundary setting (Section 2) by using the considerations outlined above, and conduct numerical tests of the scheme by applying it to a limited-area, 11-level PE model in the prediction of a Haurwitz-type wave (Section 3).

2. Formulation of the scheme

a. Strategy

We assume a situation in which slowly moving long waves are the predominant disturbances near the lateral boundary. In order to make the above assumption valid, we need to damp high-frequency waves, if excited within the domain, before they propagate to the boundary. This can be done by various means. A frequency-selective, time-integration method (Kurihara and Tripoli, 1976) was used in the present study. We consider that quantities near the boundary propagate with the local wind. Therefore, to determine whether a gridpoint is a point of inflow or outflow for the waves propagating through the boundary, the direction of the local wind component normal to the boundary was used. Thus, that point would be called an inflow or outflow (boundary) point. The same definition was used by Ross and Orlanski (1982).

We specify the tangential component of the wind at the inflow boundary points and the normal component at all boundary points. Since the local wind is inward (outward) at the inflow (outflow) boundary points, the above condition corresponds to one of the specifications which passed both the theoretical and experimental stability tests for integrating the shallow-water equations (Elvius and Sundström, 1973). It was adopted in a baroclinic model by Okamura (1975).

In the present formulation, the above boundary conditions are implemented with a technique which is analogous to the one employed by Cho and Clark (1981) in treating the normal velocity at the inflow boundary points. The prediction of the wind is first made at the boundary points using the information of the inner domain only. Next, the obtained values are relaxed toward the prescribed boundary values through a damping technique. In order to perform the first stage of the above two-step procedure in our model, we need to specify the values at the outer open side of the boundary boxes containing the boundary gridpoints. The conditions to determine these values will be called the open side conditions. If we apply a simple extrapolation formulation to obtain the open side values, the above prediction stage may cause irregularity of fields at the boundary. However, the boundary values predicted from the first stage are constantly adjusted toward the prescribed values at each second stage. A large deterioration of the boundary values is thus avoided.

The scheme mentioned above may seem similar to the one proposed by Davies (1976). However, significant differences exist between the two. Davies considered analytical studies concerning the well-posedness of the boundary conditions (e.g., Charney, 1962; Elvius and Sundström, 1973) to be disparate from development of pragmatic techniques. All variables are specified at the boundary points in his scheme. We think that the results of the analytical studies for simple cases can still be utilized in complex cases. Hence, in our scheme, a constraint at the boundary is placed on a subset of variables. Another difference is that the relaxation of the fields to a specified reference state is made in a boundary zone in Davies' scheme, whereas it is done only at the boundary points in the present scheme. We note here that a boundary zone is also used in the scheme proposed by Perkey and Kreitzberg (1976), in which the model-determined tendency is linearly combined with the tendency specified at the boundary.

As mentioned before, the amplitudes of gravity waves near the boundary are supposedly small in our case. Then, assuming that the flow at the boundary is nearly geostrophic, we can estimate the temperature gradient normal to the boundary from the vertical shear of the tangential component of wind through the thermal wind relation. This is a unique feature of our boundary setting. Due to this constraint, the temperature at an inflow point is specified not independently but by a diagnostic formula. At an outflow point, the same formula serves as an extrapolation scheme for temperature.

In the formulation of lateral boundary conditions, special care is required in the treatment of the winds in the planetary boundary layer. Otherwise, inertia waves of large amplitude can be excited. We apply an appropriate diagnostic formula to the boundary gridpoints to determine the boundary layer wind. As to the boundary layer temperature field near the lateral boundary, a barotropic state is simply assumed.

In the following, some details of our scheme are described. Although the formulation is made for a non-staggered, uniform longitude–latitude grid system in the present study, it may be possible to devise a similar scheme for a staggered grid system as well. For the convenience of description, we consider the northern boundary of a limited-area domain. There should be no difficulties in writing the formulas for the other three boundaries. Fig. 1 shows the configuration of gridpoints near the northern boundary. Points C and C–1 indicate the position of a boundary

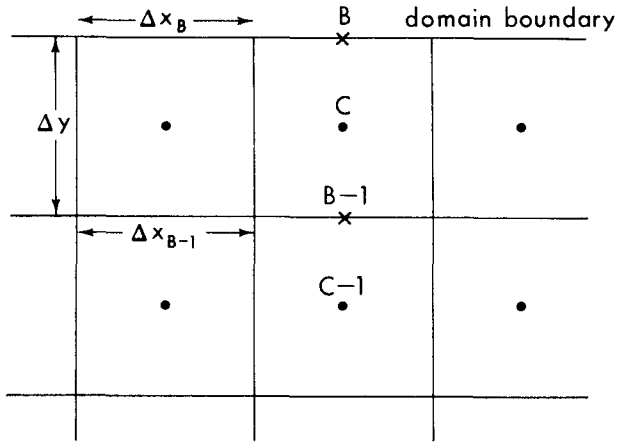

FIG. 1. Positions of the boundary gridpoint C, the gridpoint C–1 at one grid distance inside, the open side B, and the inner interface B–1 of a northern boundary box. Side length of a box is Δx_B at the north, Δx_{B-1} at the south and Δy at the west and east.

gridpoint and the one just inside of C, respectively. The open, northern side of a boundary box, which contains point C, is denoted by B, while the southern interface located at the distance Δy from the open side is designated by B–1. The above notations will be used as subscripts to indicate quantities at corresponding locations. Other notations used are σ (pressure normalized by surface value; used as the vertical coordinate), t (time), u (zonal component of wind), v (meridional component of wind), T (temperature), r (mixing ratio of water vapor), Φ (geopotential of a σ-surface), p_* (surface pressure), ρ (density at the surface), R (gas constant), f (Coriolis parameter), Δx and Δy (zonal and meridional side lengths of a boundary box, respectively), Δt (time step), k (model level index, increasing downward) and K (level index at one level above the top of the boundary layer).

b. *Open side condition*

In the present scheme, we first make the prediction of u, v, p_* and r by the box method (Kurihara and Holloway, 1967) with the use of information which is available in the computational domain. Required quantities on the open side B in Fig. 1 are obtained by the scheme presented in Table 1. The open side condition for u, v and r is based on the linear extrapolation of those quantities from points B–1 and C toward point B. The formula for p_* is derived from the assumption that the surface pressure gradient normal to the boundary is in geostrophic balance with u at level K, i.e.,

$$\frac{\partial p_*}{\partial y} = -\rho f u(K). \tag{2.1}$$

In writing (2.1), we assumed that the surface was flat. Otherwise, it is necessary to add the term $\rho g(\partial z_*/\partial y)$, where z_* is the surface height, to the left-hand side. The thermal wind relationship is assumed for the tangential component of the wind:

$$\frac{\partial T}{\partial y} = \frac{f}{R}\frac{\partial u}{\partial \ln\sigma} + \frac{\partial T}{\partial \ln\sigma}\frac{\partial \ln p_*}{\partial y}. \tag{2.2}$$

We expect (2.1) and (2.2) may be successfully used even if a boundary is chosen near the equator, although the assumption of geostrophic balance becomes weak in such a case. This is because f serves not as a divisor, but as a multiplier in the formula used to determine the mass field. The finite difference form of (2.2) yields the formula for T_B. The last term in (2.2) is related to the coordinate transformation between the pressure and the sigma system. For the levels $k \geqslant K$, $\partial u/\partial \ln\sigma$ in (2.2) is set to zero. The variables u, v, p_*, T and r at the interface B–1 are given by the average of the corresponding quantities at points C and C–1. The diffusive flux at B is determined so that the diffusive flux divergence normal to the boundary vanishes at each boundary box.

c. *Momentum at the boundary points*

We let the momentum obtained with the open side condition at the first stage be denoted by $(h^*)_c$, where h stands for either u or v. At the next stage, we use a Newtonian damping method to relax $(h^*)_c$ toward a prescribed time-dependent reference value $(h_0)_c$. The damping may be expressed as

$$\frac{\partial h}{\partial t} = -t_d^{-1}(h - h_0), \tag{2.3}$$

where t_d is the relaxation time. Denoting an advanced time level by the superscript $\tau + 1$, estimating the

TABLE 1. Open side conditions, or values at Point B in Fig. 1.

Variable	Scheme
p_{*B}	$p_{*B-1} - [fu(k = K)]_c \rho_c \Delta y$
T_B	$T_{B-1} + \frac{1}{R}\left[f\frac{\partial u}{\partial \ln\sigma}\right]_c \Delta y + \left[\frac{\partial T}{\partial \ln\sigma}\right]_c \ln\frac{p_{*B}}{p_{*B-1}}$; $k < K$
	$T_{B-1} + \left[\frac{\partial T}{\partial \ln\sigma}\right]_c \ln\frac{p_{*B}}{p_{*B-1}}$; $k \geqslant K$
Φ_B	Derive from T_B through the hydrostatic relation
v_B	$2v_C - v_{B-1}$
$(p_*v)_B$	$p_{*B}v_B$
$(p_*vu)_B$	$(p_*v)_B(2u_C - u_{B-1})$
$(p_*vv)_B$	$(p_*v)_B v_B$
$(p_*vr)_B$	$(p_*v)_B(2r_C - r_{B-1})$
(Diffusive flux)$_B$	(Diffusive flux)$_{B-1}(\Delta x)_{B-1}/(\Delta x)_B$

left-hand side by $(h^{\tau+1} - h^*)/\Delta t$ and the right-hand side by $-(h^{\tau+1} - h_0)/t_d$, and measuring t_d in the unit of Δt, i.e., $t_d = A\Delta t$, we obtain the formula

$$(h^{\tau+1})_C = \frac{1}{1+A}[(h_0)_C + A(h^*)_C]. \quad (2.4)$$

The damping is applied to both u and v at inflow points and to only v, i.e., the normal component, at outflow points. (Note that setting the damping coefficient A to a very large value is equivalent to eliminating the relaxation of the boundary point values to the prescribed ones.) Whether the gridpoint C is an inflow or outflow point is determined by the direction of v_{C-1}. The four corner points of the domain are always considered inflow points. The reference value h_0 may be derived from a previous integration of a larger domain coarse mesh model or specified by other means. In particular, a formula to determine the boundary layer winds is presented in Appendix B.

d. Temperature at the boundary points

The temperature at point C is obtained diagnostically through the finite-difference form of the thermal wind relation (2.2):

$$T_C = T_{C-1} + \frac{1}{R}\left[f\frac{\partial u}{\partial \ln\sigma}\right]_{B-1}\Delta y + \left[\frac{\partial T}{\partial \ln\sigma}\right]_{B-1}\ln\frac{(p_*)_C}{(p_*)_{C-1}}. \quad (2.5)$$

We use (2.5) for the levels higher than level K, i.e., $k < K$. For $k \geq K$, $\partial u/\partial \ln\sigma$ in (2.5) is ignored. At the four corner points of the domain, T_C is determined from the average of values calculated along the zonal and meridional directions respectively.

e. Surface pressure and mixing ratio of water vapor at the boundary points

The predictions of p_* and r at the boundary grids are made through the use of the open side condition.

3. Numerical test

a. The numerical model

The numerical model used for the test of the proposed lateral boundary setting was the 11-level PE model constructed at the Geophysical Fluid Dynamics Laboratory (GFDL), NOAA. The governing equations and the computational schemes used are explained in the paper by Kurihara and Bender (1980) for their nested mesh model. For the test cases presented here, the number of nests was reduced to one uniform nest, consisting of 37 × 37 boxes of 1° longitude–latitude resolution with the gridpoints located at the centers of the boxes. The southern and the northern boundaries of the domain were placed at 2.5°N and 39.5°N, respectively.

The lateral boundary conditions described in the preceding section were applied to the above-mentioned regional model. The level index K was set to 7, implying that level 8 ($\sigma = 0.895$) was approximately at the top of the boundary layer. The density ρ in (2.1) was determined by $(\sigma_{11}p_*)/(RT_{11})$, where the suffix 11 indicates values at level 11 ($\sigma = 0.992$; altitude of ~68 m). The constant A which represents the damping time scale in (2.4) was fixed at 5 for levels 1–5, and 10 for levels 6–11.

As mentioned before, the computational scheme proposed by Kurihara and Bender (1980) was employed in the present experiment. Their scheme involves a Newtonian-type damping for smoothing the flow field within six grid points from the lateral boundaries. It should be noted here that the reference value, which is similar to h_0 in (2.4), in the above damping is not prescribed but obtained from the values at the surrounding grid points. The damping coefficients used were also identical to the parameters n mentioned in their paper.

b. Experimental design

The test of the scheme was conducted in a 48 h prediction of the propagation of a Haurwitz-type wave. The analytical solution is known for a nondivergent, barotropic Haurwitz wave. We assumed such a solution could be taken as an approximate, though not exact, solution for the waves in the present experiment. Accordingly, it was utilized for examination of the integration results as well as for prescription of the boundary reference values. We carried out the integrations of the model for the following two cases.

CASE 1:

The model included neither moisture nor the effect of surface friction. The initial flow field was derived at all levels from the following streamfunction (Phillips, 1959) which expresses a Haurwitz wave on a sphere:

$$\psi = -a^2\omega\sin\phi + a^2\kappa\cos^m\phi\sin\phi\cos m\lambda, \quad (3.1)$$

where a is the radius of the earth, λ the longitude and ϕ the latitude. The zonal wavenumber was set equal to 10, i.e., $m = 10$. The constants ω and κ were chosen to be -1.6×10^{-6} s^{-1} and 4.05×10^{-7} s^{-1}, respectively. The wind components u and v were obtained from $u = -(1/a)\partial\psi/\partial\phi$ and $v = (1/a\cos\phi)\partial\psi/\partial\lambda$, respectively. In the present PE model, the initial mass field which was in balance with the wind field was obtained by the procedure explained in Appendix A.

In Fig. 2, the initial wind field derived from (3.1)

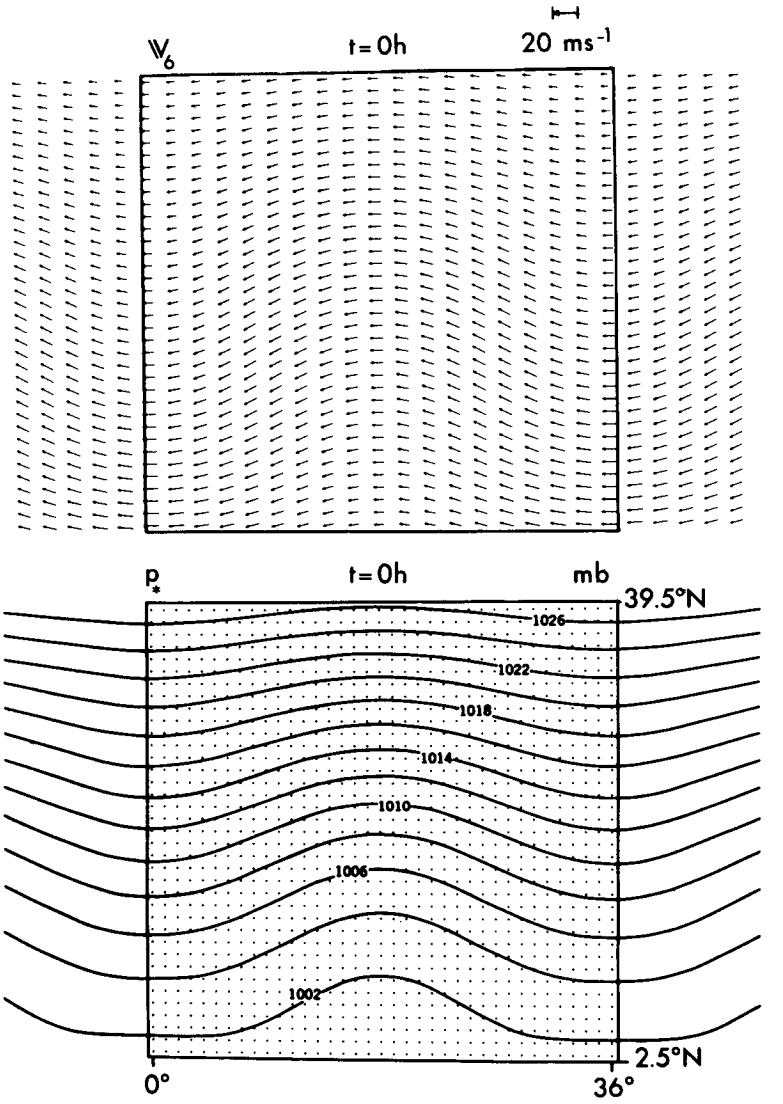

FIG. 2. Distribution of wind vectors at level 6 (top) and surface pressure (bottom) at the initial time. The framed area indicates the limited area domain for the integration.

at level 6 as well as the balanced initial surface pressure field are presented. Waves outside of the integration domain can move into the model only through a properly specified time-varying boundary condition.

If the long wave specified by (3.1) is treated in the non-divergent barotropic case, it should propagate zonally with the angular velocity (e.g., Phillips, 1959)

$$\nu = \frac{m(3+m)\omega - 2\Omega}{(1+m)(2+m)}, \qquad (3.2)$$

where Ω is the angular velocity of the earth. For the constants used in this study, Eq. (3.2) yields a westward propagation speed of ~ 10 m s^{-1}. The model integrations of Case 1 were performed with two different specifications of reference values. In the one integration, which we call Exp. 1A, the reference values of momentum at the boundary points were derived from (3.1) with its zonal phase being shifted at the angular velocity (3.2). In the other integration, i.e., Exp. 1B, the above-mentioned translation speed was slowed down to 80% of (3.2); this was done deliberately to test the scheme's behavior when a somewhat inaccurate boundary condition is imposed.

CASE 2:

Both the effect of surface friction and the hydrologic cycle, including the latent heat release due to the condensation of water vapor, were incorporated

in the model. The sea surface temperature was fixed at 302 K. The initial wind and mass fields were the same as those in Case 1, except that the wind in the planetary boundary layer was modified by the scheme explained in Appendix B. The initial relative humidity used was the same as described in the paper by Kurihara and Tuleya (1974). Two model integrations, i.e., Exps. 2A and 2B, were performed, starting from the above initial condition. The specification of the time-varying reference values at the boundary points during the two time integrations were the same as those for Exps. 1A and 1B, respectively, except that the reference winds in the boundary layer were calculated by the formula in Appendix B.

c. *Results of the experiments*

The numerical model used in the above-mentioned Case 1 should behave like a shallow water equation model unless internal inertia-gravity waves are excited. Therefore, the proposed boundary setting, which is proper for a shallow water equation system, was expected to produce a smooth numerical result. In particular, if the specified boundary values were fairly accurate, then the obtained solution will remain nearly exact for an entire domain; this was the case expected for Exp. 1A.

The wind vectors at level 6 (σ = 0.665) and the distribution of surface pressure in Exp. 1A after 48 h of model integration are presented in the left column of Fig. 3. The corresponding wind vector in the non-divergent barotropic case calculated from (3.1) as well as the surface pressure field balanced to it are also shown in the right column of Fig. 3. The results indicate that the fields in Exp. 1A vary smoothly from the inner area toward the boundary. The propagation of the long waves in Exp. 1A was very similar to that in a non-divergent barotropic case. It should be noted again that the reference values specified at the boundary points in Exp. 1A were taken from the analytical solution for the non-divergent barotropic case. The amplitude of the waves were well maintained during the 48 h integration.

In contrast to Exp. 1A, Exp. 1B is characterized by an inaccurate specification of the reference values at the boundary points. The results from Exp. 1B for the same quantities as shown for 1A are presented in the middle column of Fig. 3. The distortion of the wave phase due to inaccurate information at the inflow points is evident in the eastern third of the do-

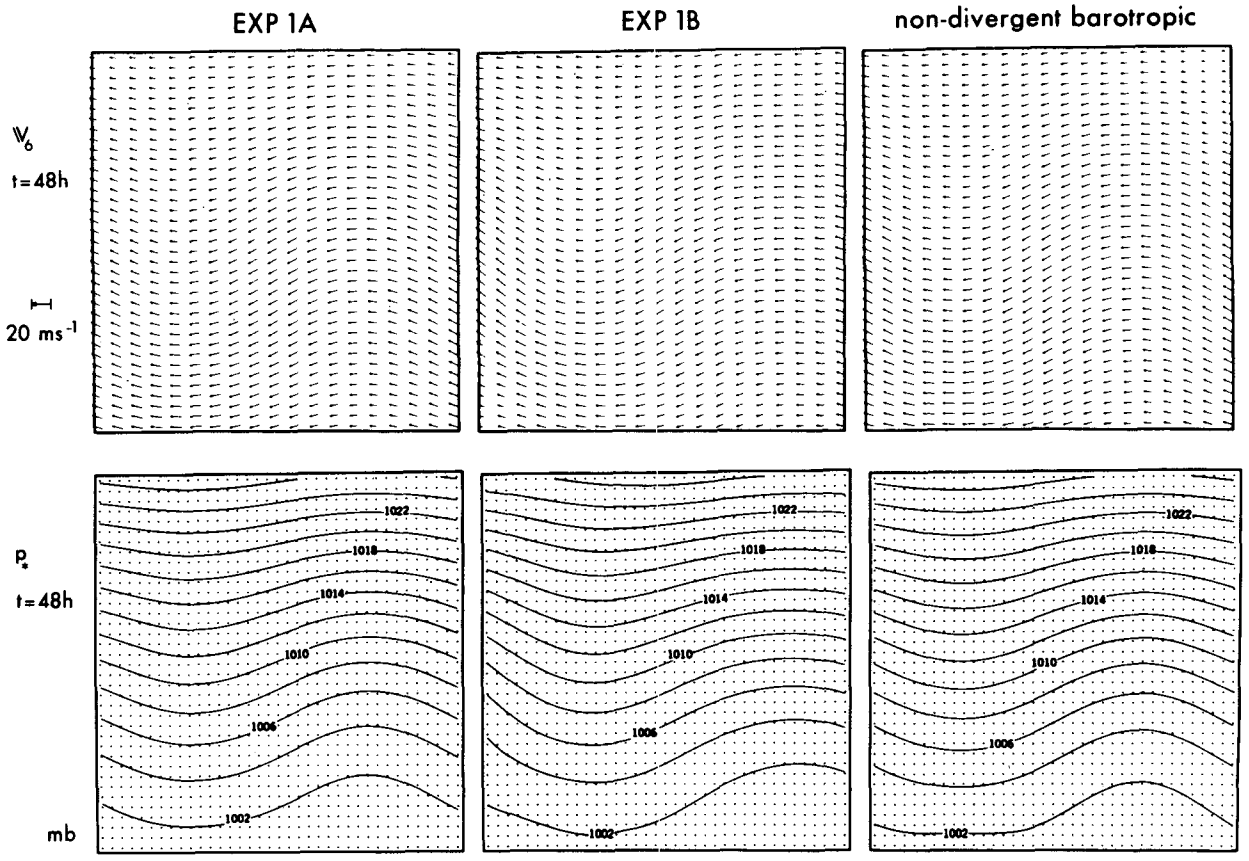

FIG. 3. Distribution of wind at level 6 (upper row) and surface pressure (lower row) after 48 h integration in Exps. 1A (left column) and 1B (middle), and the analytical solution at 48 h in nondivergent barotropic case (right).

main. The amplitude of the wave is slightly reduced near the eastern edge of the domain. It is important to note that the fields obtained after the 48 h integration were smooth and, that the effect of inaccurate boundary specification did not appear beyond the distance the waves were advected from the inflow boundary.

In the Case 2 experiment, which included the effects of surface friction as well as the hydrological process, the scheme to treat the boundary layer wind at the boundary could be tested. The results from Exps. 2A and 2B at 48 h are summarized in Fig. 4. In addition to the wind vectors at level 6 and the surface pressure distribution, the wind vectors at level 11 (σ = 0.992) are presented in order to show the behavior of the boundary layer wind. The wind vectors at level 6 vary quite smoothly between the inner region and the boundary points. The wind pattern in Exp. 2A shows very good resemblance to the solution for the non-divergent case (the upper right figure in Fig. 3). The level 11 wind fields in both experiments maintained patterns coherent to the level 6 winds during the integration period, except that small distortion occurred at the outflow points for the tangential component of the wind. The shape of the surface pressure wave was also well maintained in both experiments, although once again the amplitude was slightly damped at the inflow area in Exp. 2B. The surface friction caused a small difference in the mass flux across the northern and the southern boundaries, resulting in a loss of mass on the order of a millibar a day throughout the integration domain. We do not know if such a change is reasonable or not.

4. Summary and remarks

A scheme was formulated to treat the open lateral boundary of a limited-area primitive equation model. It is assumed that gravity waves do not prevail in the vicinity of the open boundary. Some features of the proposed scheme are as follows: 1) the degree of overspecification of the boundary condition is kept low—in particular, it is avoided in the absence of internal gravity waves; 2) the thermal wind relationship is used to specify the mass field near the boundary; 3) winds at the boundary gridpoints are not replaced abruptly by the specified reference values, but damped gradually toward them; and 4) special care is taken to treat the planetary boundary layer.

Numerical tests of the scheme were conducted with

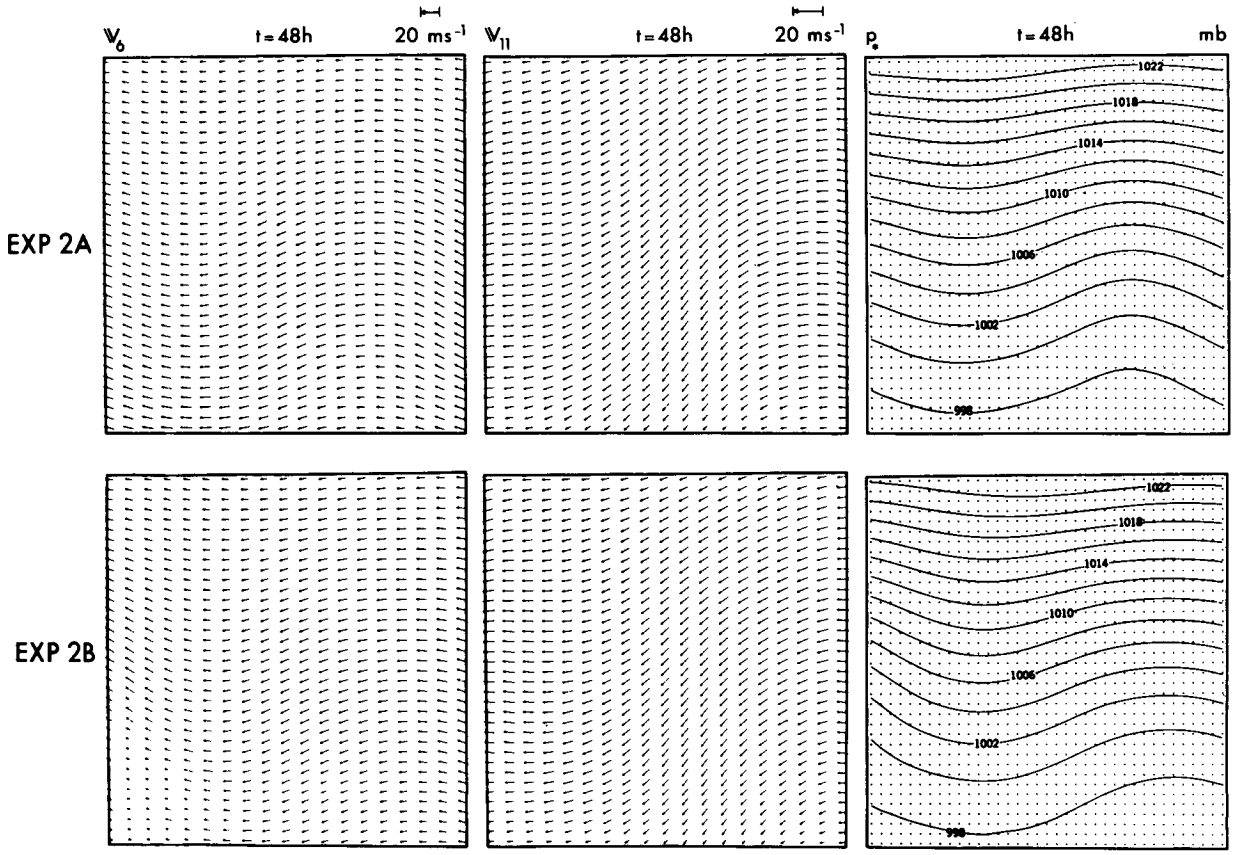

FIG. 4. Distribution of wind at level 6 (left column), wind at level 11 (middle) and surface pressure (right) after 48 h integration in Exps. 2A (upper row) and 2B (lower row).

an 11-level limited-area model in which a Haurwitz-type wave was specified at the initial time. Two cases, i.e., one without the effects of moisture and surface friction and the other including both of these effects, could be integrated smoothly for 48 h with two different sets of reference wind prescriptions for each case. This scheme has also been applied to a recent numerical simulation experiment of tropical cyclones at GFDL, and its performance so far has been satisfactory. However, since in both cases the vertical wind shear above the boundary layer was small, the use of the thermal wind relationship in the boundary specification was not strictly tested. This will be done when the model is integrated with real data in future experiments. We suspect that there may be other cases for which the open side conditions presented in Section 2 may have to be rectified. In doing so it will be useful to examine some approaches taken in the past, such as the divergence control near the boundary (Okamura, 1975), the condition on the synoptic state vertical velocity (Pielke, 1974) and the condition on the flux divergence at the boundary (Kurihara and Bender, 1980).

It should be noted that the time-dependent reference values at the boundary cannot always be prescribed. In such a case, the reference values may have to be derived from the values at one point inside the boundary gridpoints. In some of our recent experiments, the reference values thus obtained at a certain time level were kept unchanged until they were updated after an appropriate period. This practice was found to work well.

We also note that some physical constraints on the model may be imposed through the specification of the reference values. For instance, if the conservation of total mass within the domain is desired, it can be accomplished by adjusting the normal component of the wind appropriately. As mentioned in Section 3, the total mass decreased in the Case 2 integrations in the test of our scheme. Results from subsequent experiments indicate, however, that the total mass can be maintained by making a small correction, usually about several centimeters per second, to the inflow and/or outflow at the boundary.

Acknowledgments. The authors are grateful to B. Ross and R. E. Tuleya for reading the original manuscript and making valuable comments on it. They appreciate an anonymous reviewer who pointed out some of the related works. Thanks are also due to J. Kennedy for typing the manuscript and to P. G. Tunison and J. N. Conner for preparing the figures.

APPENDIX A

Specification of the Pressure Field

In the present work, the initial mass field which was balanced with the streamfunction (3.1) was obtained by the relaxation of the finite-difference reverse balance equation (see, Kurihara and Bender, 1980, Appendix B). To perform the relaxation, we have to specify p_* and Φ (geopotential of a constant σ-surface) at the boundary points of the computational domain. Formulas to compute these boundary values are derived below.

According to Phillips (1959), the pressure field which is balanced with the streamfunction (3.1) may be expressed in terms of the geopotential height H of the free surface of a barotropic model, i.e.,

$$H = H_0 + a^2A(\phi) + a^2B(\phi)\cos m\lambda + a^2C(\phi)\cos 2m\lambda. \quad \text{(A1)}$$

Constants H_0, $A(\phi)$, $B(\phi)$ and $C(\phi)$ are defined in his paper. Note that both the streamfunction and H are independent of height.

The pressure gradient force in our model must take the value ∇H. We suppose that the zonal means of surface pressure and temperature are given at the latitude ϕ_0; we denote them by $\bar{p}_*(\phi_0)$ and $\bar{T}(\phi_0, \sigma)$, respectively. If the temperature is approximated by $\bar{T}(\phi_0, \sigma)$ in the general expression for the pressure gradient force in the σ-coordinate system, we obtain

$$\nabla\Phi = \nabla H - R\bar{T}(\phi_0, \sigma)\nabla \ln p_*. \quad \text{(A2)}$$

In making the above approximation, we assume that the horizontal variation of T is not large. (The temperature field in the model was computed from Φ after the latter was obtained.) From (A2), the following approximate formula may be obtained:

$$\Phi(\lambda, \phi, \sigma) = H(\lambda, \phi) - R\bar{T}(\phi_0, \sigma)[\ln p_*(\lambda, \phi)] + E(\sigma), \quad \text{(A3)}$$

where $E(\sigma)$ is a σ-dependent constant. Taking the zonal mean of (A3) along ϕ_0 yields

$$\bar{\Phi}(\phi_0, \sigma) = \bar{H}(\phi_0) - R\bar{T}(\phi_0, \sigma)[\ln \bar{p}_*(\phi_0)] + E(\sigma). \quad \text{(A4)}$$

Through the hydrostatic relation, $\bar{\Phi}(\phi_0, \sigma)$ can be computed for a given distribution of $\bar{T}(\phi_0, \sigma)$.

From (A3) and (A4), it follows that

$$\Phi(\lambda, \phi, \sigma) - \bar{\Phi}(\phi_0, \sigma) = H(\lambda, \phi) - \bar{H}(\phi_0) - R\bar{T}(\phi_0, \sigma)\{\ln[p_*(\lambda, \phi)/\bar{p}_*(\phi_0)]\}. \quad \text{(A5)}$$

In particular, the left-hand side of (A5) vanishes at the surface, i.e., for $\sigma = 1$. Accordingly, after some manipulations, we obtain

$$p_*(\lambda, \phi) = \bar{p}_*(\phi_0)\exp\left\{\frac{a^2}{R\bar{T}(\phi_0, 1)}[A(\phi) - A(\phi_0) + B(\phi)\cos m\lambda + C(\phi)\cos 2m\lambda]\right\}. \quad \text{(A6)}$$

For any other σ-surfaces, we can easily derive

$$\Phi(\lambda, \phi, \sigma) = \bar{\Phi}(\phi_0, \sigma) + R\bar{T}(\phi_0, 1)\left[1 - \frac{\bar{T}(\phi_0, \sigma)}{\bar{T}(\phi_0, 1)}\right] \ln\left[\frac{p_*(\lambda, \phi)}{\bar{p}_*(\phi_0)}\right]. \quad \text{(A7)}$$

We specify p_* and Φ at the domain boundary by utilizing (A6) and (A7).

APPENDIX B

Specification of Boundary Layer Winds

As mentioned in the text, the winds in the planetary boundary layer are obtained in a diagnostic manner at the initialization of the model and also at the specification of the reference winds at the boundary gridpoints during the time integration of the model. The boundary layer winds within the computational domain are predicted after the initial time.

To derive a diagnostic formula, we postulate that the winds below height D are expressed for each point by

$$if\{\mathbf{v}(z) - \mathbf{v}(D)\} = K_m \frac{\partial^2 \mathbf{v}}{\partial z^2}, \quad \text{(B1)}$$

where $i = \sqrt{-1}$, $\mathbf{v}(z) = u(z) + iv(z)$, $f\mathbf{v}(D)$ represents the pressure gradient force independent of height, and K_m denotes an eddy diffusion coefficient. Note that, for $D \to \infty$, $\mathbf{v}(\infty) \to \mathbf{v}_g$ (geostrophic wind) and the condition $\mathbf{v}(0) = 0$, (B1) expresses the Ekman spiral. Since $\mathbf{v}(z) - \mathbf{v}(D)$ vanishes for $z = D$, (B1) yields

$$\mathbf{v}(z) - \mathbf{v}(D) = A\{\exp[-(1 + i)\gamma z] - \exp[-(1 + i)\gamma(2H - z)]\}, \quad \text{(B2)}$$

where A is a complex constant and $\gamma = \{f/(2K_m)\}^{1/2}$. If a logarithmic wind profile is assumed for $z < h$ ($h < D$), then the condition for $\mathbf{v}$ can be set at $z = h$ as

$$\mathbf{v}(h) = h \ln \frac{h}{z_0}\left(\frac{\partial \mathbf{v}}{\partial z}\right)_h. \quad \text{(B3)}$$

The subscript h in (B3) indicates the value at the height h and z_0 is the roughness length. Determining A from (B2) and (B3), we can derive the following diagnostic formula after somewhat lengthy manipulation:

$$\left.\begin{aligned} u(z) &= m(z)u(D) + n(z)v(D) \\ v(z) &= -n(z)u(D) + m(z)v(D) \end{aligned}\right\}. \quad \text{(B4)}$$

The quantities $m(z)$ and $n(z)$ in (B4) are

$$\left.\begin{aligned} m(z) &= 1 - d_1 \cos\lambda_1 + d_2 \cos\lambda_2 \\ n(z) &= d_1 \sin\lambda_1 - d_2 \sin\lambda_2 \end{aligned}\right\},$$

with

$$\left.\begin{aligned} d_1 &= d_1(z) = b_0 \exp\{-\gamma z\} \\ d_2 &= d_2(z) = b_0 \exp\{-\gamma(2H - z)\} \\ \lambda_1 &= \lambda_1(z) = \theta_0 - \gamma z \\ \lambda_2 &= \lambda_2(z) = \theta_0 - \gamma(2H - z) \end{aligned}\right\}.$$

In the above expressions, b_0 and θ_0 are given by

$$b_0 = (b_1^2 + b_2^2)^{-1/2} \quad \text{and} \quad \theta_0 = \tan^{-1}(b_2/b_1),$$

where

$$\left.\begin{aligned} b_1 &= a_1 \cos\theta_1 + a_2 \cos\theta_2 - a_3 \cos\theta_3 + a_4 \cos\theta_4 \\ b_2 &= a_1 \sin\theta_1 + a_2 \sin\theta_2 - a_3 \sin\theta_3 + a_4 \sin\theta_4 \end{aligned}\right\},$$

with

$$\left.\begin{aligned} &\theta_1 = \gamma h, \quad \theta_2 = \theta_1 - (\pi/4), \quad \theta_3 = \gamma(2H - h) \\ &\theta_4 = \theta_3 - (\pi/4) \\ &a_1 = \exp(-\theta_1), \quad a_2 = \sqrt{2}c\gamma a_1, \quad \text{where} \\ &c = h \ln(h/z_0) \\ &a_3 = \exp[-\gamma(2H - h)] \quad \text{and} \quad a_4 = \sqrt{2}c\gamma a_3 \end{aligned}\right\}.$$

In the present study, the approximate heights of levels 8 and 11 were taken for D and h, respectively, i.e., $D = 926$ m and $h = 68$ m. In practice, the level 8 wind was used for $v(D)$ and the winds at the lower σ-levels were approximated by those derived from (B4) at the heights appropriately assigned for the respective levels. Also, z_0 and K_m were set equal to 0.05 cm and 5 m^2 s^{-1}, respectively.

REFERENCES

Béland, M., and T. Warn, 1975: The radiation condition for transient Rossby waves. *J. Atmos. Sci.*, **32**, 1873–1880.

Busalacchi, A. J., and J. J. O'Brien, 1980: The seasonal variability in a model of the tropical Pacific. *J. Phys. Oceanogr.*, **10**, 1929–1951.

Charney, J. G., 1962: Integration of the primitive and balance equations. *Proc. Int. Symp. Numerical Weather Prediction*, Tokyo, Meteor. Soc. Japan, 131–152. [Japan Meteorological Agency, Chiyoda-ku, Tokyo, 100, Japan.]

Chen, J. H., 1973: Numerical boundary conditions and computational modes. *J. Comput. Phys.*, **13**, 522–535.

——, and K. Miyakoda, 1974: A nested grid computation for the barotropic free surface atmosphere. *Mon. Wea. Rev.*, **102**, 181–190.

Cho, H.-R., and T. L. Clark, 1981: A numerical investigation of the structure of vorticity fields associated with a deep convective cloud. *Mon. Wea. Rev.*, **109**, 1654–1670.

Davies, H. C., 1976: A lateral boundary formulation for multilevel prediction models. *Quart. J. Roy. Meteor. Soc.*, **102**, 405–418.

Elvius, T., 1977: Experiments with a primitive equations model for limited area forecasts. *Contrib. Atmos. Phys.*, **50**, 367–392.

——, and A. Sundström, 1973: Computationally efficient schemes and boundary conditions for a fine-mesh barotropic model based on the shallow-water equations. *Tellus*, **25**, 132–156.

Hack, J. J., and W. H. Schubert, 1981: Lateral boundary conditions for tropical cyclone models. *Mon. Wea. Rev.*, **109**, 1404–1420.

Klemp, J. B., and D. K. Lilly, 1978: Numerical simulation of hydrostatic mountain waves. *J. Atmos. Sci.*, **35,** 78–107.

Kurihara, Y., and J. L. Holloway, Jr., 1967: Numerical integration of a nine-level global primitive equation model formulated by the box method. *Mon. Wea. Rev.*, **95,** 509–530.

——, and R. E. Tuleya, 1974: Structure of a tropical cyclone developed in a three-dimensional numerical simulation model. *J. Atmos. Sci.*, **31,** 893–919.

——, and G. J. Tripoli, 1976: An iterative time integration scheme designed to preserve a low-frequency wave. *Mon. Wea. Rev.*, **104,** 761–764.

——, and M. A. Bender, 1980: Use of a movable nested-mesh model for tracking a small vortex. *Mon. Wea. Rev.*, **108,** 1792–1809.

Miyakoda, K., and A. Rosati, 1977: One-way nested grid models: The interface conditions and the numerical accuracy. *Mon. Wea. Rev.*, **105,** 1092–1107.

Okamura, Y., 1975: Computational design of a limited-area prediction model. *J. Meteor. Soc. Japan,* **53,** 175–188.

Orlanski, I., 1976: A simple boundary condition of unbounded hyperbolic flows. *J. Comput. Phys.*, **21,** 251–269.

Perkey, D. J., and C. W. Kreitzberg, 1976: A time-dependent lateral boundary scheme for limited-area primitive equation models. *Mon. Wea. Rev.*, **104,** 744–755.

Pielke, R., 1974: A three-dimensional numerical model of the sea breezes over South Florida. *Mon. Wea. Rev.*, **102,** 115–139.

Phillips, N. A., 1959: Numerical integration of the primitive equations on the hemisphere. *Mon. Wea. Rev.*, **87,** 333–345.

Ross, B. B., and I. Orlanski, 1982: The evolution of an observed cold front. Part I: Numerical simulation. *J. Atmos. Sci.*, **39,** 296–327.

Sundström, A., 1977: Boundary conditions for limited-area integration of the viscous forecast equations. *Contrib. Atmos. Phys.*, **50,** 218–224.

——, and T. Elvius, 1979: Computational problems related to limited-area modeling. *GARP Publ. Ser.*, No. 17, WMO, 379–416.